An effective color image segmentation approach using superpixel- neutrosophic C-means clustering and gradient-structural similarity

Bin Ji, Xuedong Hu, Feng Ding, Yunyun Ji, Han Gao

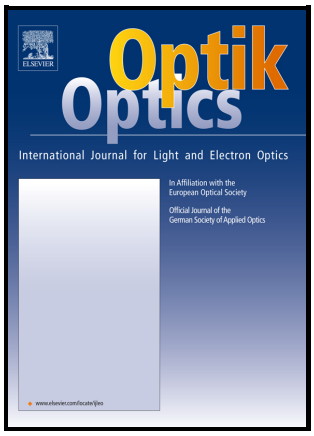

PII: S0030-4026(22)00409-0

DOI: https://doi.org/10.1016/j.ijleo.2022.169039

Reference: IJLEO169039

To appear in: *Optik*

Received date: 20 January 2022
Revised date: 19 March 2022
Accepted date: 3 April 2022

Please cite this article as: Bin Ji, Xuedong Hu, Feng Ding, Yunyun Ji and Han Gao, An effective color image segmentation approach using superpixel-neutrosophic C-means clustering and gradient-structural similarity, *Optik,* (2022) doi:https://doi.org/10.1016/j.ijleo.2022.169039

An effective color image segmentation approach using superpixel- neutrosophic C-means clustering and gradient-structural similarity

Bin Ji [a, *], Xuedong Hu [a], Feng Ding [a], Yunyun Ji [a], Han Gao [a]

[a]*Anhui University of Technology, Department of Computer Science and Technology, Ma'anshan 243032, China*

**Corresponding Author, E-mail: 1042891880@qq.com*

Abstract: Due to the insufficient expression of uncertain information in fuzzy sets, the fuzzy C-means clustering algorithm is difficult to deal with clustered boundary and outliers. Therefore, this paper proposes a color image segmentation method based on neutrosophic C-means clustering. First, we improved the simple linear clustering algorithm to obtain accurate and natural adaptive local spatial neighborhoods. Secondly, local neighborhood information is added to the objective function of neutrosophic C-means clustering to obtain a more accurate membership. According to the membership, superpixels are divided into certainty group and uncertainty group. Finally, the certainty group is classified by the maximum membership, and the superpixels of the uncertain group are classified by the structural similarity. Experimental results show that the proposed method has better performance on clean and noise images.

Keywords: color image segmentation, neutrosophic C-means clustering, superpixel, structure similarity

1. Introduction

Color is an important information medium, which can be used in many fields such as remote sensing and medical treatment. The additional color information makes image processing and analysis closer to the real situation. Image segmentation is an important part of image analysis. Most of these image segmentation methods divide the image into uniform, disjoint, and meaningful regions based on grayscale, spatial texture, and geometric features. Compared with the segmentation method that only uses grayscale, color is an important quantity to improve the quality of segmentation [1]. But the image is complicated due to the noise, background, and uneven intensity, so in order to cope with the above situations, different image segmentation methods have been produced.

At present, color image segmentation methods mainly include threshold segmentation, region growing, cluster analysis, neural network, and so on [2-5]. Among them, the clustering algorithm is a method of statistics and analysis of classification, and the essence of image segmentation is to classify pixels with similar features [6]. Therefore, clustering is closely related to image segmentation, and clustering algorithms have many applications in image segmentation [7-9], such as K-means clustering algorithm, hierarchical clustering algorithm, fuzzy C-means clustering algorithm, spectral clustering algorithm etc. Among many clustering techniques, the unsupervised fuzzy C-means clustering proposed by Bezdek [10] has been widely used in the field of image segmentation due to its iterative implementation, low storage cost, and high execution efficiency [11].

Fuzzy C-means clustering (FCM) algorithm is one of the representatives of clustering methods based on the objective function. But the algorithm only relies on information such as pixel grayscale and is more sensitive to noise and background in practical applications. For this reason, scholars have proposed a variety of improved FCM algorithms that combine local spatial information. Ahmed et al. introduced the neighborhood spatial constraint information of pixels into the objective function, and obtained a new fuzzy C-means clustering algorithm (FCMS) based on spatial constraints [12]. On this basis, the literature [13] proposed FCMS1 and FCMS2, which use mean filtering and median filtering to obtain spatial neighborhood information, respectively.

Since both the average filtered image and the median filtered image can be calculated before the start of the iteration phase, the calculation cost is lower than FCMS. The literature [14] proposes an FCM algorithm based on a hidden Markov random field, through the hidden Markov random field to obtain neighborhood information to affect the classification of the target pixel. Krinidis and Chatzis proposed a robust fuzzy local information C-means clustering (FLICM) algorithm [15], which defines a new fuzzy local neighborhood factor that can automatically determine the spatial and gray relationship, and add it to the objective function to ensure anti-noise and image detail preservation. But the above algorithms all use fixed-size spatial distances, and are not robust to different local information and noise. Lei et al. proposed a fast and robust FCM (FRFCM) algorithm [16], which uses multivariate morphological reconstruction to fuse the local spatial information into the FRFCM but does not add the neighborhood information to the objective function. On this basis, the literature [17] combined morphology and watershed algorithm to obtain a superpixel image with adaptive areas, and added the neighborhood information of the superpixel image to the objective function. But it is too much affected by the gradient.

Although the improved FCM algorithm considers the neighborhood information of the image, but the fuzzy set only uses membership to express the positive information that an element belongs to the set, and lacks the sufficient ability to express uncertain information. Therefore, in order to make up for the lack of fuzzy theory, scholars introduce neutrosophy theory [18] into clustering algorithms and apply it to image segmentation. GUO et al. proposed the neutrosophic C-means clustering (NCM) algorithm, which makes full use of the advantages of the neutrosophic theory, effectively clusters boundary and noise, and improves accuracy of classification [19]. But neutrosophic C-means clustering has the same problem as FCM that does not contain spatial information. The literature [20] proposed the IFNCM algorithm, which defines an indeterminacy filter to obtain the neighborhood information after filtering, but the fixed size of the filter window makes the algorithm less robust.

From the above analysis, NCM algorithm using neutrosophic theory to improve FCM algorithm can effectively deal with boundary pixels and outliers in the clustering process. And for the problem that NCM algorithm does not contain any spatial information, combined with the improved method of FCM algorithm, we propose a superpixel-neutrosophic C-means clustering with gradient-based structural similarity algorithm and apply it to color image segmentation. The improved superpixel segmentation algorithm is used to obtain superpixel images with more natural contours, and the NCM algorithm with neighborhood information is used to cluster the superpixel images. According to the membership, the superpixels are divided into definite and uncertain groups. The superpixels of the definite group will be directly classified by the maximum membership, and the superpixels of the uncertain group will be classified according to the global spatial information and structural similarity (brightness, Contrast, gradient). The experimental results show that the proposed algorithm can obtain more effective segmentation results whether on clean or noise images.

The rest of this paper is organized as follows. Section 2 introduces the related background. Section 3 elaborates the proposed method. Section 4 presents the experimental results and discusses the experimental results. Conclusion are made in Section 5.

2. Related backgrounds

2.1. Simple linear clustering algorithm

Superpixels in image segmentation refer to irregular pixel blocks with similar texture, color, brightness, and other characteristics that are similar to each other. Superpixel images use a small number of superpixels instead of a large number of pixels to express image features, so it is usually used as a preprocessing step in segmentation algorithms. These superpixel algorithms are roughly divided into two categories [21], one is based on graph theory, and the other is based on gradient ascent. Among them, the simple linear clustering (SLIC) algorithm [22] is more widely used because of its obvious advantages in time complexity, boundary recall rate, and segmentation error rate.

The SLIC algorithm first converts the image from the original RGB color space to the CIELab color space, which is generally considered as perceptually uniform for smaller color distances, and then combines the three components of the CIELab color space with the position information of the pixels in the image to construct a five-dimensional feature C as follows.

$$C_i = [l_i, a_i, b_i, x_i, y_i]^T \tag{1}$$

Where l is Luminosity, a and b are two color channels. x and y are the pixel coordinates, i is the subscript of the pixel.

$$d_{lab} = \sqrt{\left(l_k - l_i\right)^2 + \left(a_k - a_i\right)^2 + \left(b_k - b_i\right)^2} \tag{2}$$

$$d_{xy} = \sqrt{\left(x_k - x_i\right)^2 + \left(y_k - y_i\right)^2} \tag{3}$$

The main work of SLIC is to use Eq. (2) and (3) to calculate the similarity between pixels for local clustering. d_{lab} is the color distance between pixels. d_{xy} is the Euclidean distance between pixels, and k is the subscript of the clustering centers. The steps of the SLIC algorithm are as follows:

Step 1. Initialization of seed points:

Assuming that the input image has N pixels, the step size is s, and the step size s represents the distance between the center points of the two initial local clusters, which is mainly used to control the size of superpixels. Then, roughly N/s^2 superpixels are expected to be obtained after calculation, and the SLIC algorithm will generate a grid with the step size s as Fig.1(a), and set center points (seed points) of the initial local cluster in each cell as shown in the red circle in Fig. 1(a). When the SLIC algorithm selects these seed points, in order to prevent the seed point from falling into the edge of the image, it will find the pixel with the smallest gradient in the 3×3 neighborhood of the initial center as the new seed point.

Step 2. Calculate the similarity:

Within the given search range, calculate the similarity $D(i,k) = \sqrt{{d_{lab}}^2 + [(m/s)d_{xy}]^2}$ between each pixel and the seed point according to Eq. (2) and (3).

Step 3: Form superpixels:

According to the similarity measurement result, keep the pixel category consistent with the category of the seed point with the highest similarity. Repeat step 2 and 3 until the clustering result does not change significantly or reaches the required number of iterations.

Step 4: Enforce connectivity:

Reallocate discontinuous or too small superpixels to neighboring superpixels.

But in the process of dividing the grid and determining the seed point in step 1, the edge width of the image is not one pixel wide, then reselected seed points may still fall on the edge of the image, and the SLIC algorithm only searches within the 2S range of the seed points for computational efficiency during local clustering as Fig. 1(b). Then there will be a situation as Fig.1(c), the edge pixels of the image can only be searched and calculated within the domain $2S \times 2S$, which leads to the edges of some superpixels that do not fit the original image.

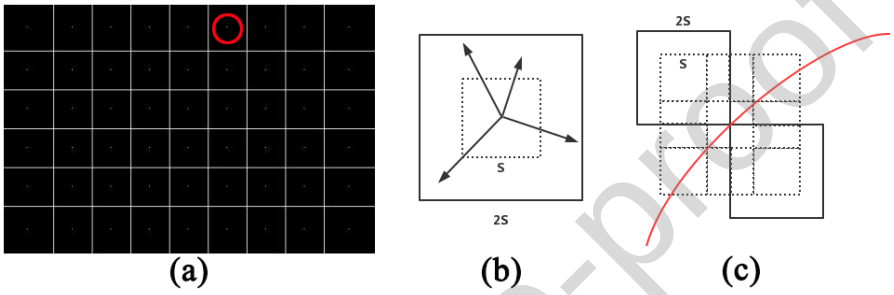

Fig. 1. (a) The initial grid and seed points(image size is 267×400, S =45). (b)SLIC searches a limited region. (c)Seed point fall on the edge.

2.2. Neutrosophic C-means clustering

In cluster analysis, the traditional fuzzy clustering can only describe the degree of certainty that the samples belong to each group. But in fact, the samples at the boundary between different groups are difficult to determine which group they belong to. In order to solve this problem, Guo et al. introduced the neutrosophic set into the fuzzy clustering algorithm and proposed the neutrosophic C-means clustering (NCM) algorithm [19]. Redefine the set of all samples as the union of the definite set and the uncertain set. Let $A = C_j \cup B \cup R, j = 1, 2, ..., n$ where is the set of all samples, C_j is an determinant cluster, B regards the cluster in boundary regions, R is associated with noisy data and $\cup$ is the union operation. B and R are two kinds of indeterminate clusters. T is defined as the degree of definite collection, I is the degree of boundary collection, and F is the degree of noise collection. Considering the uncertainty of clustering, define a new objective function and degree of membership as:

$$J_{NCM}(T, I, F, c) = \sum_{i=1}^{N}\sum_{j=1}^{C}\left(w_1 T_{ij}\right)^m \left\|\left(x_i - c_j\right)\right\|^2 + \sum_{i=1}^{N}\left(w_2 I_i\right)^m \left\|\left(x_i - c_{i\max}\right)\right\|^2 + \sum_{i=1}^{N}\left(w_3 F_i\right)^m \delta^2 \tag{4}$$

$$c_{i\max} = \left(c_{p_i} + c_{q_i}\right)/2 \tag{5}$$

$$p_i = \arg\max_{j=1,2,...,C}\left(T_{ij}\right) \tag{6}$$

$$q_i = \arg\max_{j \neq p_i \cap j=1,2,...,C}\left(T_{ij}\right) \tag{7}$$

In above equations, w_1, w_2, w_3 is the weight factor. m is a constant that controls the degree of ambiguity. p_i and q_i are the cluster numbers with the biggest and second biggest value of T. When the p_i and q_i are identified, the $c_{i\max}$ is calculated and its value is a constant number for each data point, and will not change any more. δ is used to control the number of objects considered as outliers.

To increase the robustness of NCM to noise, the noise distance is added to the objective function instead of δ. The noise clustering algorithm (NC) [23] considers noises as an independent class. It regards the noise distance, representing the distance between the sample point and the center of the noise cluster, as a constant. It is a key parameter that is critical to the performance of noise clustering. Based on this argument, a simplified statistical average is used to calculate δ [23]:

$$\delta^2 = \gamma \frac{\sum_{i=1}^{N}\sum_{j=1}^{C} d_{ij}^2}{NC} \tag{8}$$

where γ is a noise multiplier used to adjust the effect of noise distance, d_{ij} represents the Euclidean distance between the sample x_i and the cluster center c_j, N is the number of clustering, C is the number of clustering center. According to the conditions, we can get the formulas for calculating c_k, T_{ij}, I_i and F_i as follows:

$$c_k = \sum_{i=1}^{N}(w_1 T_{ij})^m x_i \Big/ \sum_{i=1}^{N}(w_1 T_{ij})^m \tag{9}$$

$$T_{ij} = \frac{K}{w_1}\left(x_i - c_j\right)^{-2/(m-1)} \tag{10}$$

$$I_i = \frac{K}{w_2}\left(x_i - c_{i\max}\right)^{-2/(m-1)} \tag{11}$$

$$F_i = \frac{K}{w_3}\delta^{-2/(m-1)} \tag{12}$$

where $K = \left[\sum_{j=1}^{C}\frac{1}{w_1}\left\|\left(x_i - c_j\right)\right\|^{-(2/m-1)} + \frac{1}{w_2}\left\|\left(x_i - c_{i\max}\right)\right\|^{-(2/m-1)} + \frac{1}{w_3}\delta^{-(2/m-1)}\right]^{-1}$. It can be seen from the above formula. The addition of the noise distance realizes the adaptation of δ but the objective function of the NCM algorithm still does not contain the neighborhood space information.

2.3. Gradient-based structural similarity

Gradient-based structural similarity (GSSIM) [24] is a similarity measure extended from SSIM [25]. It usually evaluates the similarity between images based on three aspects: brightness, contrast, and gradient. For brightness comparison, we use the following function $l(x, y)$:

$$l(x,y)=\frac{2\mu_x\mu_y+C_1}{\mu_x{}^2+\mu_y{}^2+C_1} \quad (13)$$

$$C_1=(K_1L)^2 \quad (14)$$

where μ_x and μ_y are the average brightness of x and y images, the constant C_1 is included to avoid instability when $\mu_x{}^2+\mu_y{}^2$ is very close to zero. C_1 is calculated by K_1 and L, where L is the dynamic range of the pixel values (255 for 8-bit grayscale images), and $K_1 << 1$ is a small constant.

For contrast comparison, we use the function $c(x,y)$:

$$c(x,y)=\frac{2\sigma_x\sigma_y+C_2}{\sigma_x{}^2+\sigma_y{}^2+C_2} \quad (15)$$

where σ_x and σ_y are the standard deviations of the brightness of x and y images, $C_2=(K_2L)^2$ and $K_2 << 1$.

For gradient comparison, we use the function $g(x,y)$:

$$g(x,y)=\frac{2g_xg_y+C_3}{g_x{}^2+g_y{}^2+C_3} \quad (16)$$

$$g_x=\max\{\Delta_0 f_x(i,j),\Delta_{90} f_x(i,j)\} \quad (17)$$

$$g_y=\max\{\Delta_0 f_y(i,j),\Delta_{90} f_y(i,j)\} \quad (18)$$

Where $\Delta_0 f_x(i,j)$, $\Delta_{90} f_y(i,j)$ are the horizontal and vertical gradients in the image at the $(i,j)th$ pixel of the image. $C_3=(K_3L)^2$ and $K_3 << 1$.

$$GSSIM(x,y)=\left[l(x,y)\right]^{\alpha}\left[c(x,y)\right]^{\beta}\left[g(x,y)\right]^{\lambda} \quad (19)$$

After we compare the brightness, contrast, and gradient between two superpixels through Eq (13), (15), and (16), the three comparisons are combined using Equation (19) to obtain GSSIM. Where $\alpha>0$, $\beta>0$ and $\lambda>0$ are parameters used to adjust the relative importance of the three components. In order to simplify the calculation, it is generally taken as 1. The larger the GSSIM value obtained, the smaller the difference between the two super pixel blocks.

3. Proposed method

3.1. Superpixel image by the improved SLIC algorithm

Superpixel images can provide better local spatial information than neighboring windows of fixed size and shape. But the superpixel image generated by the traditional SLIC algorithm will destroy the contour of the original image in some cases. To make the SLIC algorithm have better processing for the image contour, we combine the SLIC algorithm with the watershed algorithm which has a better response to the image edges.

The watershed algorithm is a fast image segmentation algorithm that calculates the local minimums of the gradient image and searches for the watershed line between adjacent local minimums. But the traditional watershed algorithm is susceptible to noise and excessive useless minima. To solve this problem, the watershed algorithm based on morphological gradient reconstruction (MMGR-WT) [17] is a simple and effective algorithm to overcome over-segmentation, which can remove noise and useless gradient details while retaining the contour details of the target. MMGR-WT uses morphological open operators to reconstruct gradient images. the open operation is a morphological operation that first performs morphological dilation reconstruction on the gradient image, and then performs morphological erosion on the reconstructed gradient image, is defined as

$$R^C(g) = R^{\varepsilon}\left(R^{\delta}(g)\right) \tag{20}$$

where R^{δ} is the morphological expansion operation, R^{ε} is the morphological corrosion operation, g is the marker image. Compared with erosion and dilation, the open operation R^C has a stronger ability to extract features and reduce noise.

It can be seen from Fig.2, MMGR-WT uses structuring elements of different sizes to obtain multiple reconstructed images in the reconstruction process, and calculates the pointwise maximum of the two reconstructed images by Eq. (5) to update the gradient image until the error of the gradient image is less than a minimum value as Eq. (6), among them, the structural elements are used as disk. Thus, the problem of over-segmentation of the original watershed algorithm is solved. The setting of this minimum value solves the problem of different maximum structural elements sizes that need to be used in different images. The final gradient image retains important edge details while removing most of the useless local minima.

$$R_f^{MC}(g, r_1, r_2) = \vee\left\{\mathrm{R}_f^C(g)_{B_{r_1}}, \mathrm{R}_f^C(g)_{B_{r_1+1}}, ..., \mathrm{R}_f^C(g)_{B_{r_2}}\right\} \tag{21}$$

$$\max\left\{R_f^{MC}(g, r_2-1, r_2) - R_f^{MC}(g, r_2, r_2+1)\right\} \le \eta \tag{22}$$

Where R^{MC} is a MMGR operation, B is the structural element, r_1 and r_2 are the minimum and maximum sizes, g is the mark image, and f represents the original gradient image. η is a constant between 0 and 1. The symbol $\vee$ represents the pointwise maximum.

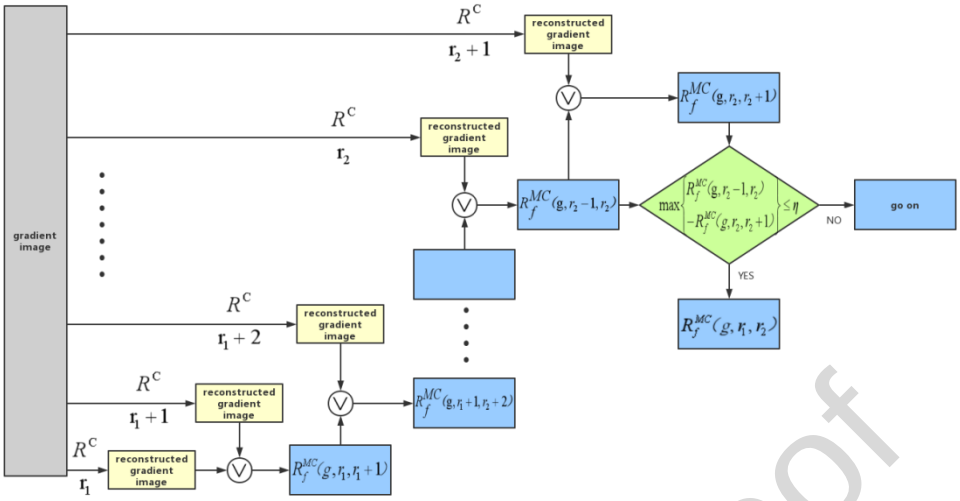

Fig. 2. The process of multiple morphological reconstruction

The improved SLIC algorithm divides the original image into multiple regions with smooth gradients based on the gradient image generated by MMGR-WT before meshing the original image, which avoids the direct processing of gradient information by SLIC. Then the SLIC algorithm generates grids and initial cluster centers in these regions, respectively, and calculates the color distance and position distance of pixels in these regions as:

$$d_{nlab} = \sqrt{\left(l_{nk} - l_{ni}\right)^2 + \left(a_{nk} - a_{ni}\right)^2 + \left(b_{nk} - b_{ni}\right)^2} \tag{23}$$

$$d_{nxy} = \sqrt{\left(x_{nk} - x_{ni}\right)^2 + \left(y_{nk} - y_{ni}\right)^2} \tag{24}$$

Where n is the subscript of the region, d_{nlab} is the color distance between pixels in the nth region, and d_{nxy} is the positional distance between pixels in the nth region. The addition of MMGR-WT increases the gradient processing of the SLIC algorithm. By limiting the calculation range of pixel similarity, the improved SLIC algorithm can obtain better boundary processing capability under the same step size.

The improved SLIC algorithm is as follows:

Step1: Use watershed to divide the image into several regions $R_1, R_2, R_3, ...R_n$, and get the number of pixels in each region $S_1, S_2, ..., S_n$;

Step2: Initialization step size s, used to control the number of superpixels generated;

Step3: If the number of pixels S_n in the region R_n is less than s^2, then this region is regarded as a superpixel, otherwise, go to step 4;

Step4: Generate initial grids and initial cluster centers by s in $R_1, R_2, R_3, ...R_n$ respectively;

Step5: Within a given step size s, calculate the similarity $D_n(i,k)=\sqrt{{d_{nlab}}^2+[(m/s)d_{nxy}]^2}$ between each pixel and the seed point according to Eq. (23) and (24).

Step6: According to the similarity measurement result, keep the pixel category consistent with the category of the seed point with the highest similarity. Repeat step 5 and 6 until the clustering result does not change significantly or reaches the required number of iterations.

Step7: Reallocate discontinuous or too small superpixels to neighboring superpixels.

3.2. NCM based on superpixel

Although the original neutrosophic C-means clustering algorithm increases the processing of the boundaries, the objective function does not involve any spatial information, resulting in poor performance in dealing with noise and weak boundaries. Therefore, to improve the accuracy of segmentation and enhance the robustness to noise, it is necessary to add spatial neighborhood information to the objective function. Combined with our improved SLIC algorithm proposed in section 3.1, we can obtain better local spatial information for NCM. The average value of the color pixels in the adaptive regions of the superpixel image is used to replace each pixel in the original image, which reduces the influence of undesired factors on the final classification result and effectively reduces the computational complexity.

Aiming at the problems of the NCM algorithm, a superpixel-neutrosophic C-means clustering (SNCM) algorithm is proposed. The objective function is:

$$J(T,I,F,c)=\sum_{l=1}^{q}\sum_{k=1}^{\mathrm{C}}S_l\left(w_1T_{kl}\right)^m\left\|\left(\frac{1}{S_l}\sum_{p\in R_l}x_p-c_k\right)\right\|^2+\sum_{l=1}^{q}S_l\left(w_2I_l\right)^m\left\|\left(\frac{1}{S_l}\sum_{p\in R_l}x_p-c_{l\max}\right)\right\|^2+\sum_{l=1}^{q}S_l\left(w_3F_l\right)^m\delta^2 \tag{25}$$

$$\delta^2=\gamma\frac{\sum_{l=1}^{q}\sum_{k=1}^{C}\left\|\left(\frac{1}{S_l}\sum_{p\in R_l}x_p-c_k\right)\right\|^2}{qC} \tag{26}$$

Where l is the color level, $1\le l\le q$, q is the number of regions of the superpixel image, c_k is the cluster center, S_l is the number of pixels in the lth superpixel R_l, and x_p is the color pixel within the lth superpixel R_l, δ is a noise distance calculated by Eq.(11). T_{kl}, I_l and F_i are the membership values belonging to the determinate cluster, boundary regions and noisy data set, $0<T_{kl},I_l,F_l<1$ which satisfy with the following:

$$\sum_{k=1}^{C}T_{kl}+I_l+F_l=1 \tag{27}$$

The objective function of Eq. (25) is derived from the objective function of fuzzy clustering, and the convergence of fuzzy clustering has been discussed and proved [26]. Therefore, the convergence of Eq. (25) can be proved. According to the above conditions, the Langrangian objective function is constructed. By using

Lagrangian multipliers to minimize the objective function (see in Appendices A), we can obtain the equations of c_k, T_{kl}, I_l, F_l as follows:

$$c_k = \frac{\sum_{l=1}^{q} (w_1 T_{kl})^m \sum_{p \in R_l} x_p}{\sum_{l=1}^{q} S_l (w_1 T_{kl})^m} \tag{28}$$

$$T_{kl} = \frac{K}{w_1} \left(\frac{1}{S_l} \sum_{p \in R_l} x_p - c_k \right)^{-(2/m-1)} \tag{29}$$

$$I_l = \frac{K}{w_2} \left(\frac{1}{S_l} \sum_{p \in R_l} x_p - c_{l\max} \right)^{-(2/m-1)} \tag{30}$$

$$F_l = \frac{K}{w_3} \delta^{-(2/m-1)} \tag{31}$$

$$K = \left[\sum_{k=1}^{C} \frac{1}{w_1} \left\| \left(\frac{1}{S_l} \sum_{p \in R_l} x_p - c_k \right) \right\|^{-(2/m-1)} + \frac{1}{w_2} \left\| \left(\frac{1}{S_l} \sum_{p \in R_l} x_p - c_{l\max} \right) \right\|^{-(2/m-1)} + \frac{1}{w_3} \delta^{-(2/m-1)} \right]^{-1} \tag{32}$$

The division of samples is achieved by iterative optimization of the objective function, and the membership T_{kl}, I_l, F_l and the cluster centers c_k are updated in each iteration. The c_{lmax} is calculated according to indexes of the top two largest values of T_{kl} in each iteration. The iteration will continuous until $\max\left\{\left|T_{kl}^{(h+1)} - T_{kl}^{(h)}\right|\right\} < \varepsilon$ or the number of iterations exceeds the limit, where h is the number of iterations, ε is a constant between 0 and 1 that controls the accuracy of the result.

Fig.3 shows the result of clustering Fig.7(c) (see in section 4.2) by the SNCM algorithm. We set 2 cluster centers for Fig.7(c). The red points are uncertain samples which $I_l > F_{kl}$, and the remaining points are divided into two definite sets. Obviously, the uncertain sample is in the boundary area of the two definite sets. It is inaccurate to determine the classification of these uncertain samples only by Euclidean distance, so we will perform additional calculations on these points.

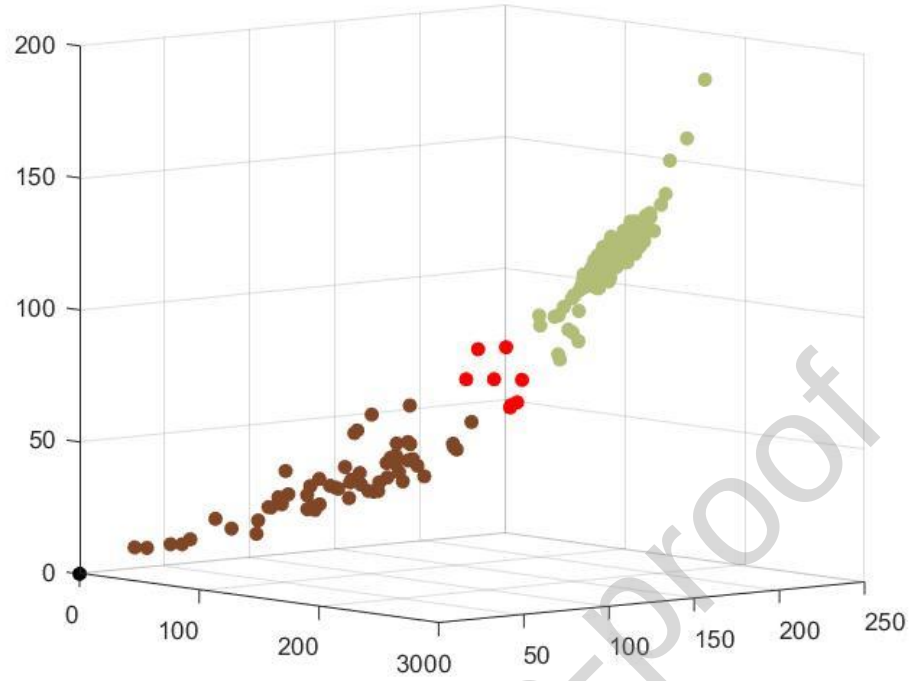

Fig. 3. Classification result of SNCM(C=2)

3.3. Superpixel-neutrosophic C-means clustering with GSSIM (SNCMWG) algorithm

The meaning of the points in the boundary set is superpixels with similar colors. When they are distinguished only by color distance, then they may be incorrectly segmented. Therefore, we hope to combine more original image information to deal with these uncertain superpixels, for this, we introduce GSSIM to compare the similarity between superpixels from the brightness, contrast, and gradient. It applies to superpixels of different sizes generated by the improved superpixel algorithm.

We take the uncertain superpixels as the target images $x_1, x_2, ..., x_n$. And as shown in the Fig.4, in order not to destroy the spatial information of the original image, we look for the superpixels adjacent to the target images and belong to a certain group as the contrast images $y_{n1}, y_{n2}, ..., y_{nm}$. Then use $GSSIM(x_n, y_{nm})$ to calculate the similarity between the target images and the contrast images. Finally, the target image is divided into the set to which the contrast images with the highest similarity belongs until all uncertain superpixels are classified into a certain set. The practical effect will be discussed in Section 4.3.

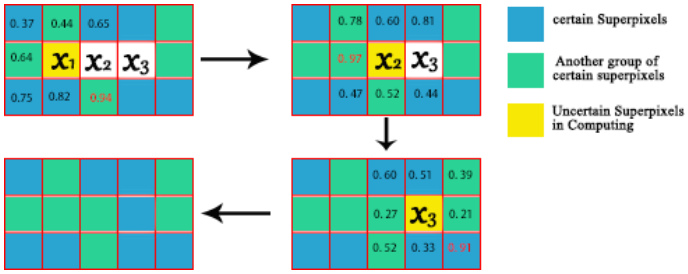

Fig. 4 Schematic diagram of assigning uncertain superpixels by GSSIM (The numbers in the figure represent the value of GSSIM).

In Section 3.1, we improved the SLIC algorithm to make the resulting superpixel image closer to the contour of the original image, and retain more image spatial information and color information. In Section 3.2, we add the spatial neighborhood information of the image to the objective function of neutrosophic clustering to obtain a more detailed and accurate membership T, I, F. And according to T and I, superpixels are divided into definite groups and uncertain groups. Superpixels belonging to a certain group will be classified directly according to the size of T, while superpixels in an undetermined group need to calculate GSSIM and determine the classification based on more original image information.

All steps in SNCMWG algorithm are summarized as follows:

Step1: initialize s, where s is used to control how many super pixels are generated;

Step2: compute a superpixel image using the improved SLIC algorithm;

Step3: initialize $T^{(0)}$, $I^{(0)}$, $F^{(0)}$ and the $c, m, \gamma, w_1, w_2, w_3$ parameters;

Step4: calculate the centers vectors $c^{(k)}$ at k step using Eq. (22);

Step5: update $T^{(h)}$ to $T^{(h+1)}$ using Eq.(23), $I^{(h)}$ to $I^{(h+1)}$ using Eq.(24), $F^{(h)}$ to $F^{(h+1)}$ using Eq.(25);

Step6: if $\left\{\left|T_{kl}^{(h+1)} - T_{kl}^{(h)}\right|\right\} < \varepsilon$ then stop; otherwise return step 4;

Step7: if the sample's $T > I$, classify the sample by T; otherwise, classify the sample by GSSIM obtained by Eq. (15);

The whole proposed process is shown in Fig. 5.

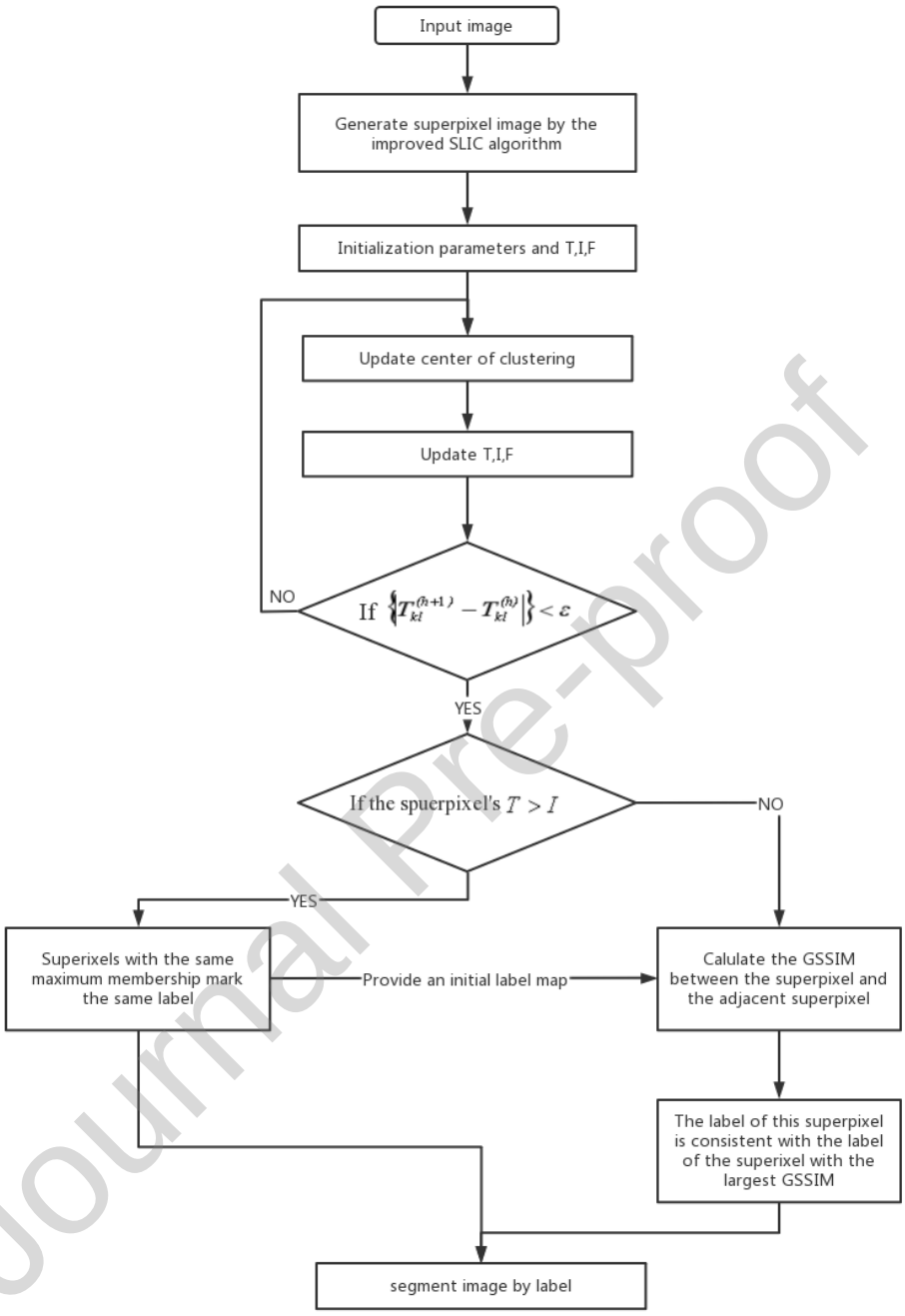

Fig. 5. The flowchart of SNCMWG algorithm

4. Experimental works and results

In this section, we will analyze the effect of the improved SLIC algorithm and the effectiveness of adding GSSIM. And in order to assess the effectiveness of SNCMWG algorithm for real image segmentation, we further conducted experiments. We compared it with FCM, NCM, FCMS2, FLICM, HMRF-FCM, FRFCM, and SFFCM algorithms. These algorithms use different methods to obtain local spatial neighborhoods in order to improve the segmentation results, and each has its advantages and disadvantages.

In the following experiment, for all methods, set the weighting exponent on the membership degree m =2, minimum error ε =0.001. A neighborhood window is unnecessary for FCM. For NCM, the following parameter w_1 = 0.7, w_1 =0.15, w_3 =0.15 and γ =0.1 are chosen for experiments. For the FCMS2, a neighborhood window of size 3×3 is used to obtain neighborhood information. In addition, median filter is used to denoise, and the filtering window is 5×5. There are no other parameters for FLICM and HMRF-FCM. For FRFCM, the structuring element used for obtaining marker image is a square of size 3×3, and the filtering window used for membership filtering is also a square of size 5×5. For SFFCM, a minimal SE of =3, and minimal error threshold r_1 =0.0001 for MMGR-WT proposed in [22]. Through a large number of experiments in the early stage, the algorithm proposed in this paper sets the minimum structure element size r_1 =2 , minimal error threshold η =0.0001 and the step size s =20 for the improved SLIC algorithm, the weight factor w_1 =0.7, w_2 =0.15, w_3 =0.15 and the noise multiplier γ =0.1 are chosen for clustering.

The EORSSD dataset is used to test the segmentation of color remote sensing images [27]. The BSDS500 [28] and MSRC [29] datasets are widely used to test the segmentation of natural images. All our experiments are performed on a machine configured with an Intel Core i5 processor, 2.3 GHz, 8 GB RAM.

4.1. Evaluation criteria

Since 2-6 cluster centers can be set for each image in BSDS500, we choose the number of cluster centers which obtains the highest PRI. And the segmentation subject is also different for each image in MSRC, therefore, we also select a segmentation subject corresponding to the highest PRI. The evaluation criteria used in this paper are given as follows:

The PRI is a similarity measure that counts the fraction of pairs of pixels whose labels are consistent between the computed segmentation S' [30], and the corresponding ground truth segmentation S . PRI can be calculated as follows:

$$PRI\left(S,S'\right)=1-\left(\sum_i\sum_j p_{ij}\right)^2-2\sum_j\left(\sum_j p_{ij}\right)^2+2\sum\sum p_{ij}^2)/N \qquad (33)$$

Where p_{ij} is the number of pixels in the i^{th} cluster of S and the j^{th} cluster of S' ,and N is the total number of pixels of the image.

The BDE is an error measure that is used to measure the average displacement error of boundary pixels between two segmentations [31]. BDE can be calculated as follows:

$$BDE\left(S,S'\right)=\left(\sum_i^{N_1}d\left(p_i,S\right)\right)/N_1+\left(\sum_i^{N_2}d\left(p_i,S'\right)/N_2\right)/2 \qquad (34)$$

Where N_1 and N_2 denote the total number of points in the boundary set S' and S , respectively. d is a distance between a pixel p_i in S' and its closest boundary pixel p in S .

The CV is an overlap measure that can be also used to evaluate the segmentation effect[28]. It is defined as:

$$CV\left(S\rightarrow S'\right)=\left(\sum_{RES}\left|R\right|\cdot\max_{R'\in S'}O\left(R,R'\right)\right)/N \qquad (35)$$

Where $O\left(R,R'\right)=\left|R\cap R'\right|/\left|R\cup R'\right|$ denotes the overlap between two regions R and R' .

The VI is a similarity measure[28], which measures the distance between two segmentations according to the average conditional entropy given by the following formula:

$$VI(S,S') = H(S) + H(S') - 2I(S,S') \tag{36}$$

Where H and I represent the entropies and mutual information between two segmentations, respectively.

When the segmentation result is close to the ground truth, PRI and CV are larger, and BDE and VI are smaller. And to evaluate the performance of different algorithms in the segmentation of noise images, the optimal segmentation accuracy (SA) and mean Intersection over Union (mIoU) are used. SA is defined as the proportion of the sum of correctly clustered pixels to the sum of all pixels, and mIoU indicates the equality of the segmented image with the ground truth value. SA and mIoU are calculated as:

$$SA = \frac{\sum_i^c A_i \cap C_i}{\sum_j^c C_j} \tag{37}$$

$$mIoU = \frac{1}{c}\sum_{i=1}^{c} \frac{A_i \cap C_i}{A_i \cup C_i} \tag{38}$$

Where A_i is the pixel set of the ith category in the segmented image, and C_i is the pixel set of the ith category in the ground truth, c is the number of cluster prototype. The larger the SA and mIoU, the more accurate the segmentation.

4.2. The effect of the improved SLIC Algorithm

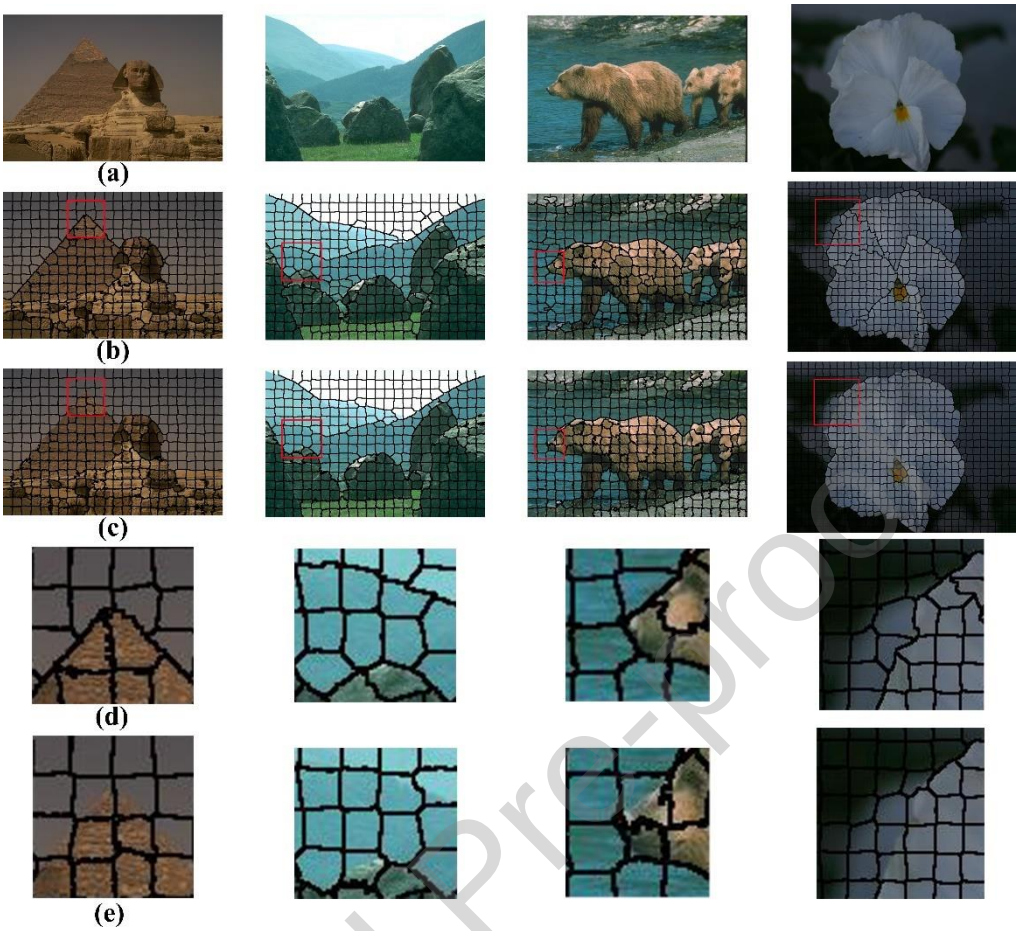

Fig. 6.Comparison of the improved SLIC algorithm and SLIC(s =20). (a) The original image. (b) Superpixel images generated by the improved SLIC algorithm. (c) Superpixel images generated by the SLIC algorithm. (d) the details of (b). (e) the details of (c).

To demonstrate the effect of the improved SLIC algorithm, Fig.6 shows the superpixel images obtained by the SLIC and the improved SLIC algorithm, respectively. It can be seen from Fig.6 (d, e) that the improved SLIC algorithm does not destroy the compactness of the original algorithm, and the generated superpixel image is closer to the contour of the original image. The improved SLIC algorithm has added MMGR-WT, which increases the processing of image contours so that the spatial information retention is more complete than the original algorithm. In addition, it can be seen from Fig.7 that the color distribution of the superpixel image is same as the original image. Therefore, when the superpixel replaces each pixel in the area, the main color information of the original image is retained, and the number of calculations required is reduced.

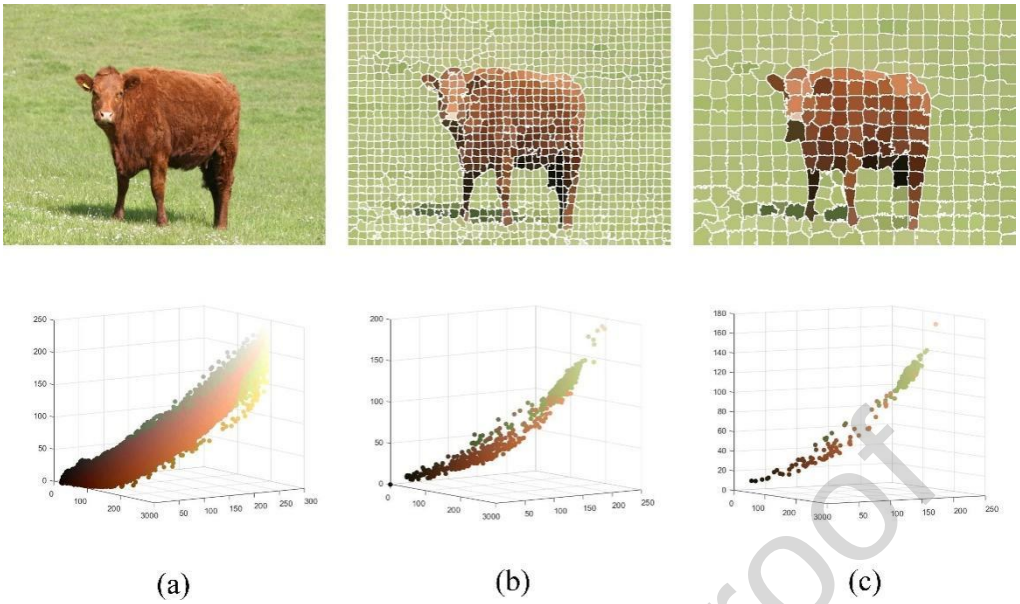

Fig. 7.The color distribution of color images. (a) The original image. (b) Superpixel images with s =15. (c)Superpixel images with s =30

4.3. The effect after adding GSSIM

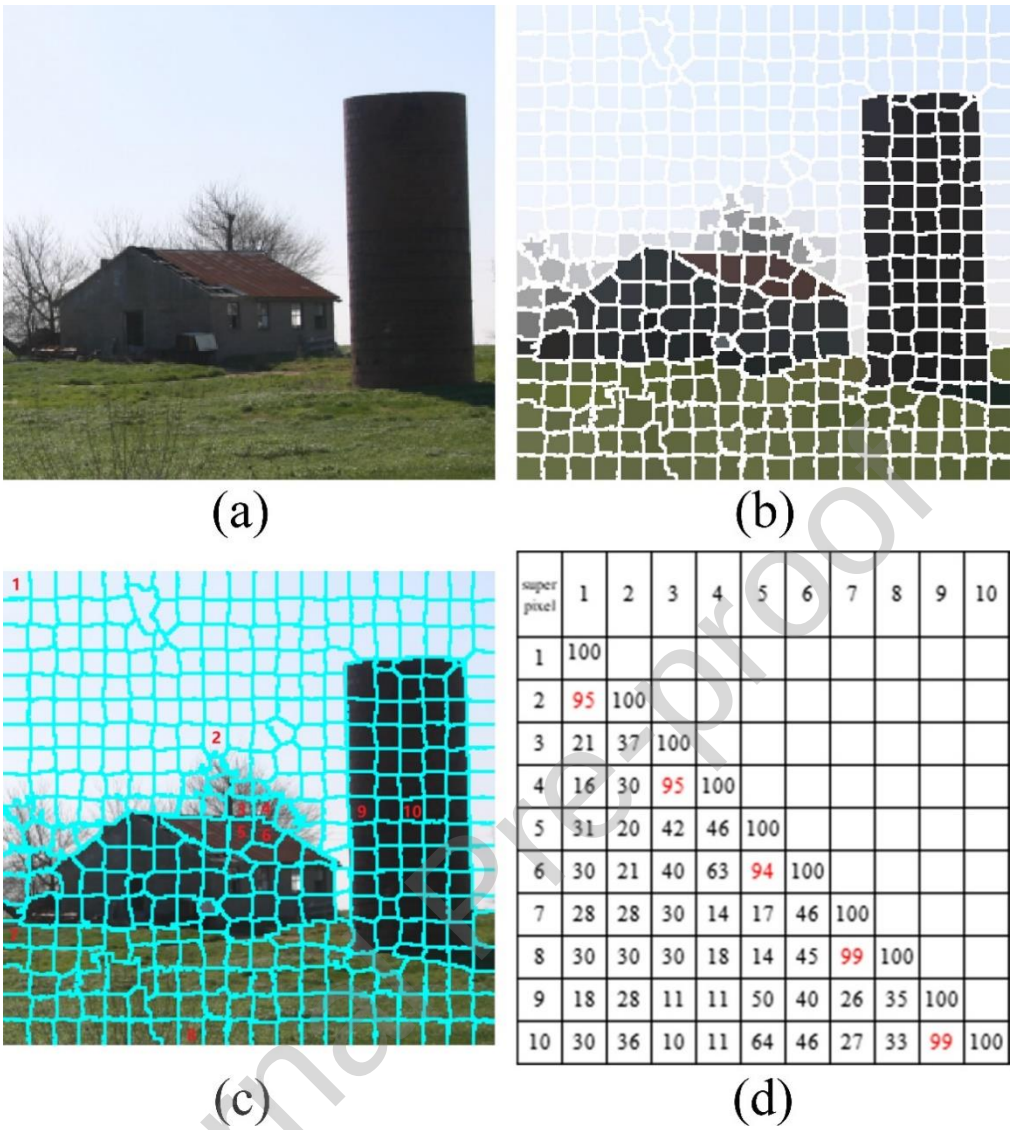

super pixel	1	2	3	4	5	6	7	8	9	10
1	100									
2	95	100								
3	21	37	100							
4	16	30	95	100						
5	31	20	42	46	100					
6	30	21	40	63	94	100				
7	28	28	30	14	17	46	100			
8	30	30	30	18	14	45	99	100		
9	18	28	11	11	50	40	26	35	100	
10	30	36	10	11	64	46	27	33	99	100

Fig. 8. The GSSIM between different superpixels. (a) The original image. (b) The superpixel image. (c) Ten superpixels in different areas. (d) The value of GSSIM between 10 superpixels(%).

We use the improved SLIC algorithm to obtain the superpixel image Fig.8(b) from (a), and select 10 superpixels from the image. Calculate and compare the GSSIM between these 10 superpixels. From Fig.8(d), we can see that the GSSIM value between superpixels in the same area is very high, such as superpixels 7 and 8. Even the colors of superpixels 3, 4, 5, and 6 are very closed, and there are obvious differences on GSSIM. Superpixels 5 and 6 belonging to the "roof" have higher GSSIM values. Superpixels 3 and 4 belonging to the "tree" also have higher GSSIM values. In addition, the GSSIM value between superpixels belonging to different natural areas does not exceed the GSSIM value between superpixels of the same natural areas.

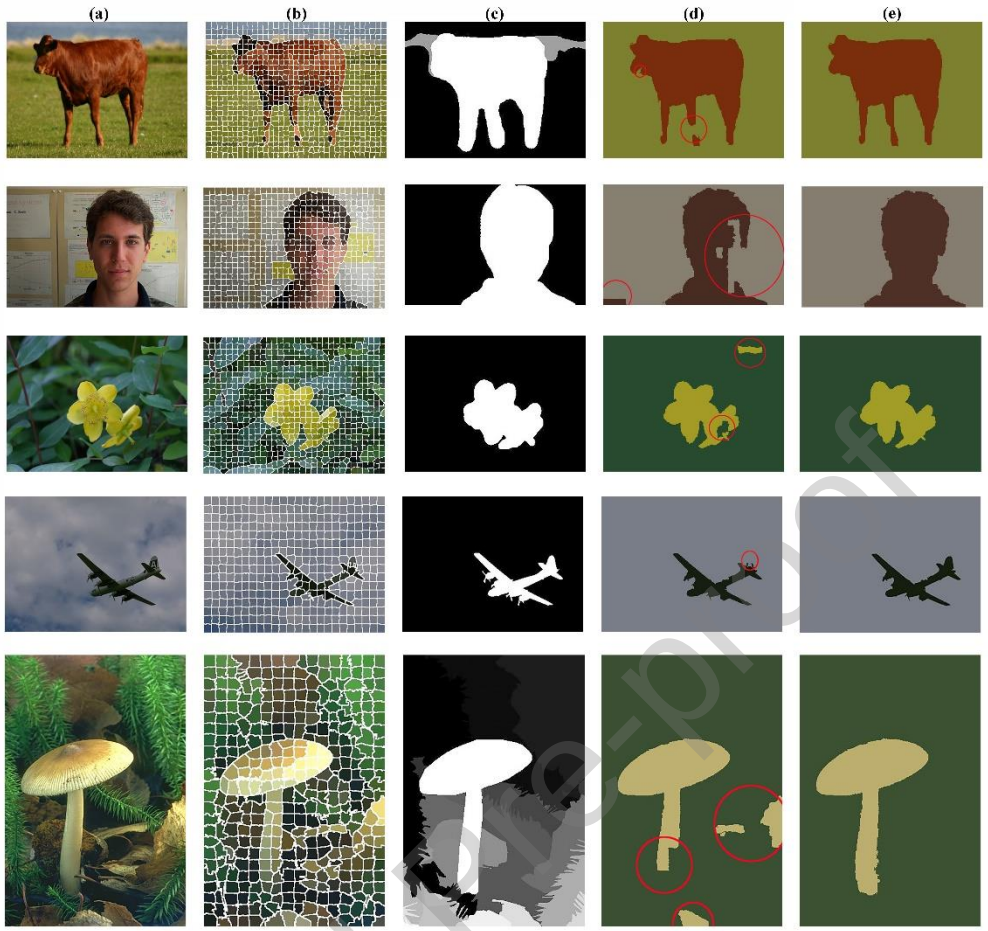

Fig. 9. Comparison of NCM with and without GSSIM. (a)The original image. (b) The superpixel image. (c)Ground Truth. (d) the segmentation results of clustering superpixel images using SNCM algorithm without GSSIM. (e) the segmentation results of clustering superpixel images using SNCM algorithm with GSSIM.

It can be seen from the Fig.9 that SNCMWG algorithm has better results than the SNCM algorithm. Since the SNCM algorithm directly classifies the image according to the maximum membership, there will be errors in segmentation in some areas with similar colors. However, the addition of GSSIM improves the accuracy of the SNCM algorithm. SNCMWG algorithm uses the membership to obtain the superpixels located in the edge area of the color space, and searches for the superpixels adjacent to these superpixels in the original image space. The SNCMWG algorithm determines the classification of these superpixels through the information of adjacent superpixels, which makes up for the deficiency of the SNCM algorithm only considering local spatial information.

4.4. Performance on clean images

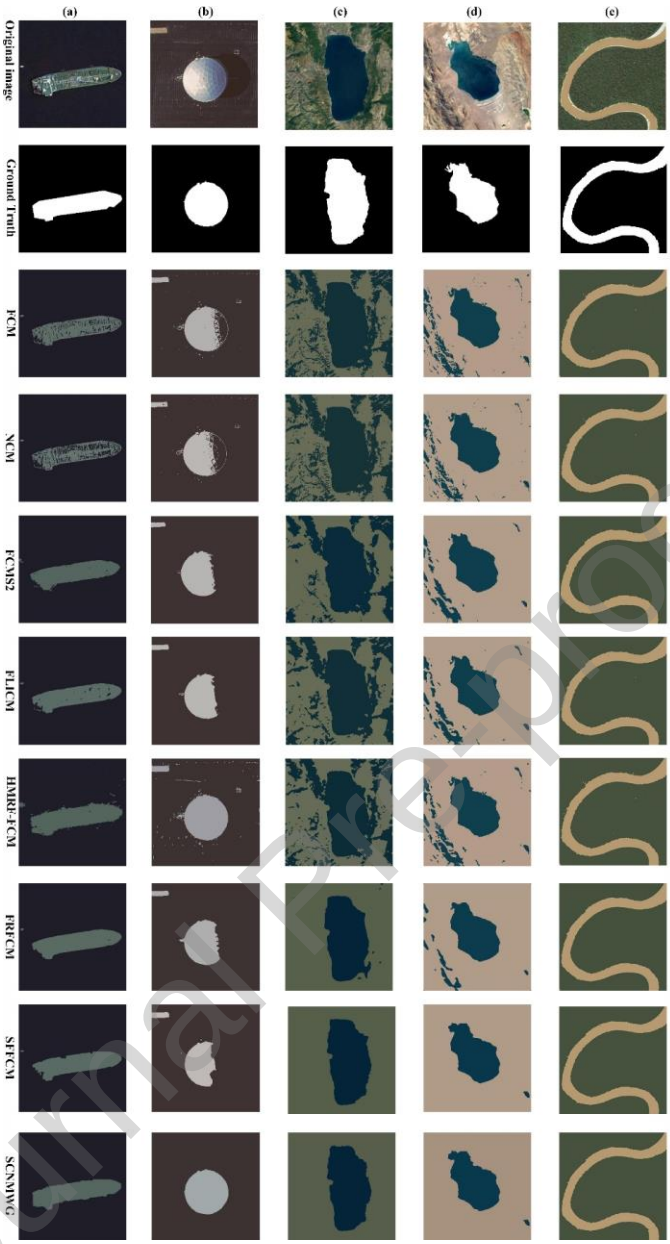

Fig. 10.Comparison of segmentation results on remote sensing images using different models. ($_C$ =2)

Fig. 10 and 11 illustrate the segmentation effect of each algorithm on clean images. Among them, Fig. 10 shows the segmentation result of the remote sensing image. For images with more complex backgrounds, FRFCM, SFFCM, and the proposed SNCMWG use adaptive domain information to obtain better results than other algorithms, as shown in Fig.10(c, d). For images with complex target colors. Except for the algorithm proposed in this paper, other algorithms have not obtained good segmentation results, as shown in Fig.10(a, b). The proposed SNCMWG uses SNCM to define areas with inconsistent colors and uses GSSIM to obtain better results.

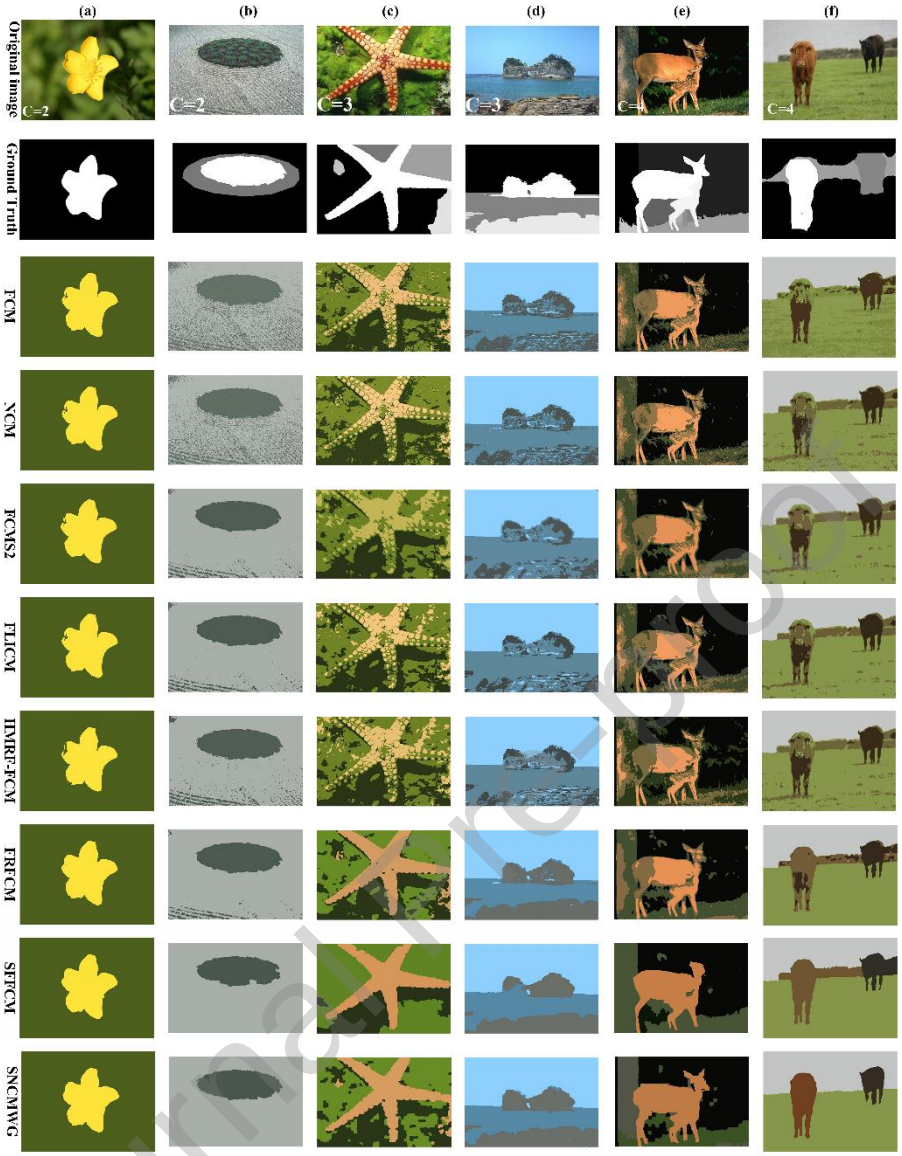

Fig. 11. Comparison of segmentation results on natural color images using different models.

Fig.11 shows the segmentation results of natural images. Since FCM and NCM algorithms do not contain spatial information, the maintenance of the target contour is poor. FCMS2, HMRF-FCM, and FLICM use a fixed spatial distance, resulting in no significant improvement in the segmentation effect. FRFCM and SFFCM achieved better results by introducing morphological reconstruction operations to obtain adaptive local spatial information. Although SFFCM uses the watershed algorithm to obtain a cleaner background than FRCFCM such as Fig.11(b, c), the watershed algorithm easily forms incorrect contours due to gradients, as shown in Fig.11(d, e). The proposed SNCMWG uses the NCM algorithm with adaptive spatial information, which obtains a more accurate classification of colors and performs better for clean images with multiple color regions, as shown in Fig.11(e, f), other algorithms confuse the target with the background, but SNCMWG obtains clear segmentation of the target.

Table 1. The average performance of eight algorithms for 100 random images on EORSSD.

Algorithms	PRI↑	CV↑	VI↓	BDE↓
FCM	0.71	0.42	3.11	14.08
NCM	0.71	0.41	3.15	13.79
FCMS2	0.74	0.40	2.74	13.60
FLICM	0.75	0.39	2.73	13.65
HMRF-FCM	0.74	0.42	2.75	13.53
FRFCM	0.75	0.43	2.48	13.17
SFFCM	0.78	0.47	2.26	13.32
SNCMWG	**0.79**	**0.55**	**2.04**	**12.17**

Table 2. The average performance of eight algorithms for 100 random images on MSRC and BSDS.

Algorithms	PRI↑	CV↑	VI↓	BDE↓
FCM	0.69	0.45	2.55	13.60
NCM	0.71	0.44	2.60	13.50
FCMS1	0.72	0.45	2.54	13.24
FLICM	0.73	0.44	2.28	13.29
HMRF-FCM	0.73	0.45	2.22	13.19
FRFCM	0.74	0.47	2.14	12.82
SFFCM	0.75	0.50	1.95	12.87
SNCMWG	**0.77**	**0.53**	**1.84**	**12.34**

The average values of PRI, BDE, CV, and VI of the segmentation results of clean images are shown in Table 1-2. It can be seen from the Table 1-2 that the PRI, BDE, CV, and VI between FCM and NCM are close. NCM algorithm is better than FCM on BDE. The segmentation effect of FCMS2, FLICM, and HMRF-FCM algorithm is better than FCM and NCM in part of PRI, BDE, CV, and VI. Due to the addition of adaptive spatial information, FRFCM and SFFCM algorithm are superior to other algorithms on PRI, BDE, CV, and VI. The proposed SNCMWG uses neutrosophic clustering with neighborhood information to cluster superpixel images, and achieves better segmentation results by introducing gradient-based structural similarity. Compared with SFFCM and FRFCM, the preprocessing time of the proposed SNCMWG is longer, but it is better than other algorithms in PRI, BDE, CV and VI.

4.5. Performance on noise images

In order to test the robustness of these comparison algorithms and the proposed algorithm in the real environment, we selected two clean color images from Section 4.3 that each algorithm achieved good segmentation results, and added Gaussian noise, Salt and pepper noise, and uniform noise to these images. The above algorithm has been implemented, and the segmentation result is shown in the Fig.12-13.

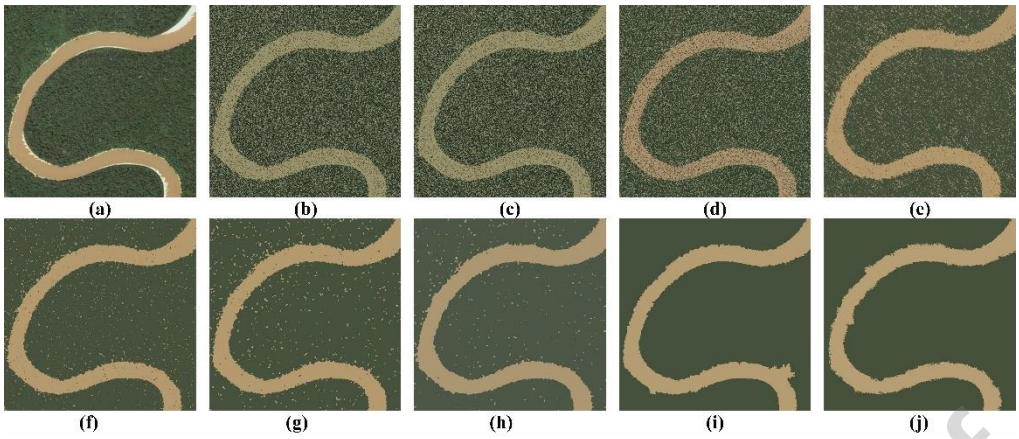

Fig. 12. Comparison of segmentation results on the remote sensing image. (a) The original image. (b) Noise image (Gaussian noise, the noise level is 10%). (c) FCM. (d) NCM. (e)FCMS2. (f) FLICM. (g)HMRF-FCM. (h)FRFCM. (i) SFFCM. (j) SNCMWG.

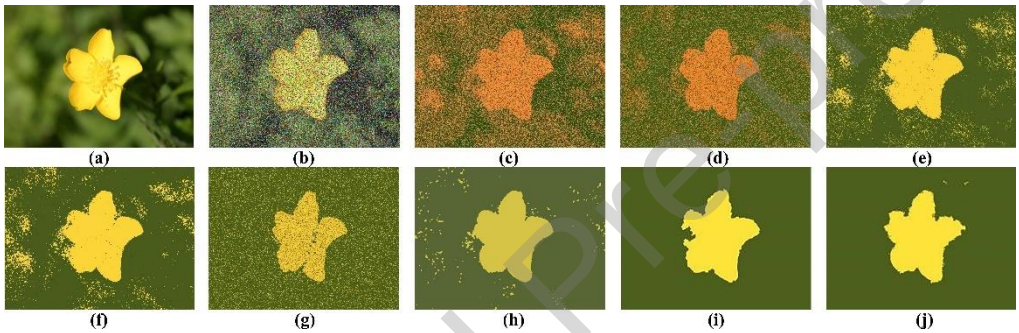

Fig. 13. Comparison of segmentation results on the natural image. (a) The original image. (b) Noise image (salt and pepper noise, the noise level is 40%). (c) FCM. (d) NCM. (e)FCMS2. (f) FLICM. (g)HMRF-FCM. (h)FRFCM. (i) SFFCM. (j) SNCMWG.

It can be seen from Fig.12-13 that FCM and NCM are not robust to noise, and the segmentation result still has a lot of noise. FCMS2 is more robust to salt and pepper noise shown in Fig.13(e). FLICM and HMRF-FCM can remove part of the noise, but they perform poorly on high-density salt and pepper noise as shown in the Fig.13(f, g). FRFCM is more robust to Gaussian noise, but it does not overcome its sensitivity to salt and pepper noise shown in Fig.13(h). According to Fig.12(i, j) and Fig.13(i, j), SFFCM and the proposed SNCMWG have better segmentation results, but the SFFCM algorithm will segment errors in some subtle areas when the noise density is high.

Table 3. A (%) comparisons of 8 methods on the remote sensing image corrupted by noise of different levels (C= 2).

Noise	FCM	NCM	FCMS2	FLICM	HMRF-FCM	FRFCM	SFFCM	SNCMWG
Gaussian 5%	79.74	80.21	87.14	99.54	99.04	99.95	99.85	99.82
Gaussian 10%	67.92	68.34	75.67	97.43	93.28	98.93	98.78	99.79
Gaussian 15%	65.11	66.51	64.23	88.31	89.25	98.84	98.54	98.69
Gaussian 20%	55.36	55.99	63.43	77.12	79.11	97.15	98.10	98.60
Salt & Pepper 10%	86.11	88.36	95.81	98.01	98.24	99.96	99.86	99.84
Salt & Pepper 20%	75.12	77.81	89.37	92.14	90.45	98.89	99.84	99.25
Salt & Pepper 35%	63.32	75.41	81.95	80.21	89.39	97.06	96.21	98.41

Salt & Pepper4 0%	55.28	56.19	74.56	78.07	79.18	96.08	95.91	98.14
Uniform 10%	77.65	78.14	83.76	99.11	99.18	99.86	99.95	99.81
Uniform 20%	66.41	66.78	72.81	97.24	96.32	99.74	99.88	99.73
Uniform 30%	55.12	56.11	62.39	85.20	84.57	99.61	99.76	99.70
Uniform 40%	54.31	54.94	61.85	76.32	64.24	98.45	98.81	98.62
Mean value	66.79	68.73	76.08	89.06	88.52	98.71	98.79	**99.20**

Table 4. SA (%) comparisons of 8 methods on the natural image corrupted by noise of different levels (C= 2).

Noise	FCM	NCM	FCMS2	FLICM	HMRF-FCM	FRFCM	SFFCM	SNCMWG
Gaussian 5%	74.10	89.48	94.13	98.89	98.07	99.21	99.89	99.80
Gaussian 10%	74.00	76.71	87.52	96.58	96.08	98.86	98.51	99.72
Gaussian 15%	70.62	73.68	72.03	94.19	92.87	97.12	98.23	98.82
Gaussian 20%	66.54	72.35	72.56	91.05	89.82	97.03	97.51	98.73
Salt & Pepper 10%	81.59	89.36	96.36	99.74	97.00	99.84	99.93	99.85
Salt & Pepper 20%	79.51	84.63	91.52	99.10	92.69	98.36	98.87	99.81
Salt & Pepper 35%	78.30	78.19	84.37	97.67	87.15	94.23	98.74	99.67
Salt & Pepper 40%	72.21	73.64	80.42	83.76	81.18	93.84	98.54	99.58
Uniform 10%	89.29	94.41	95.32	98.22	97.44	99.58	99.91	98.83
Uniform 20%	84.26	86.12	88.04	91.60	85.13	97.36	98.80	99.78
Uniform 30%	77.03	80.11	81.91	83.76	81.29	97.01	98.72	98.69
Uniform 40%	66.95	74.14	75.03	79.84	80.05	96.30	97.71	98.60
Mean value	76.20	81.07	84.93	92.87	89.90	97.39	98.78	**99.32**

It can be seen from the Fig.14 and 15 that when the noise density is low, all algorithms except FCM and NCM have good segmentation effects in mIoU. However, as the noise density increases, the segmentation effect of FCM, NCM, FCMS2, FLICM, and HMRF-FCM algorithms will decrease to varying degrees. Since FRFCM, SFFCM, and the proposed SNCMWG use adaptive neighborhood information, the value of MIOU is more stable than the above algorithm.

It can be seen from the Table 3-4 that the SA obtained by FCM2, FLICM, HMRF-FCM, FRFCM, and SFFCM with spatial domain information are higher than that of FCM and NCM algorithms. The segmentation effect of FCMS2 on salt and pepper noise images is better than other noises. The FLICM and HMRF-FCM algorithms achieved poor SA in images contaminated by salt and pepper noise or uniform noise. The segmentation effect of SFFCM and FRFCM is similar, and the segmentation effect is better for images contaminated by Gaussian noise. The proposed SNCMWG uses a superpixel algorithm based on the multivariate morphological reconstruction, which is robust to three kinds of noises and obtains the best average value of SA.

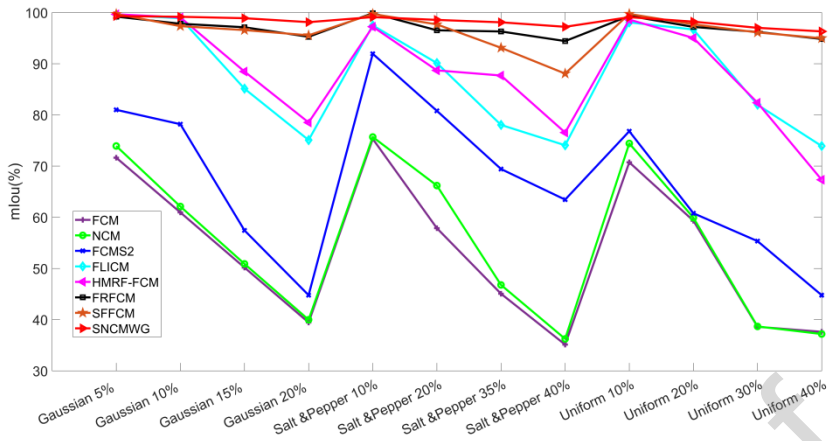

Fig. 14. mIoU (%) Graph of 8 methods to the remote sensing image corrupted by different levels of noise (C=2).

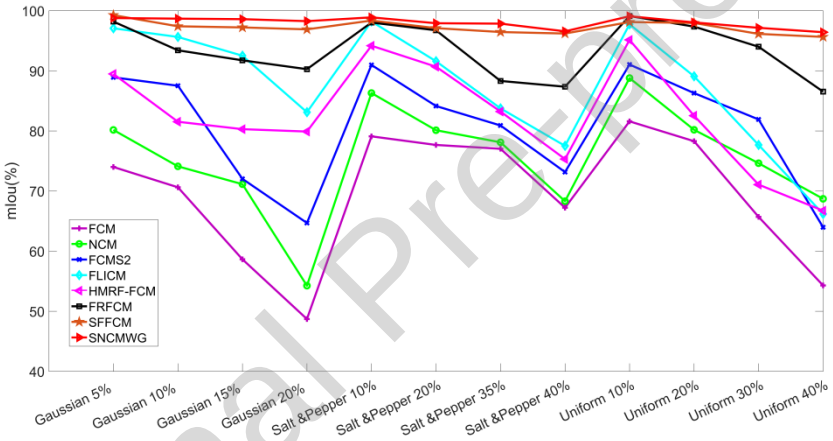

Fig. 15. mIoU (%) Graph of 8 methods to the natural image corrupted by different levels of noise (C=2).

Finally, we added a 15% mixed noise (Gaussian, Salt &Pepper and Uniform noise) level to the image. In Fig.16, we can see that because FCM and NCM do not add neighborhood information, there are still many noise pixels in the segmentation results. FCMS2 uses median filtering to suppress noise, but it only achieves a better effect on salt and pepper noise, and is not good for mixed noise with stronger randomness. HMRF-FCM uses prior probability to improve the segmentation results, but the uncertainty of noise images is high, and it is difficult to obtain appropriate prior knowledge, and the denoising effect is not good as shown in Fig.16(b). FLICM uses fuzzy local (spatial and gray) similarity measures to maintain insensitivity to noise, but the fixed-size neighborhood window makes the algorithm less robust. For FRFCM, multivariate morphological reconstruction can suppress most of the noisy pixels in the image, but there are still some noisy pixels in the rest of the area as shown in Fig.16(c). For SFFCM, the watershed algorithm based on multivariate morphological reconstruction can suppress all noise, but the watershed method is misled by the noise pixels that cannot be suppressed by morphological reconstruction, leading to incorrect segmentation of some regions such as Fig.16(a, d). Based on the multivariate morphological reconstruction, the algorithm proposed in this paper excludes noise pixels that easily cause interference from the local clustering of the SLIC algorithm. While suppressing most of the noise pixels, the main correct contour of the target is maintained.

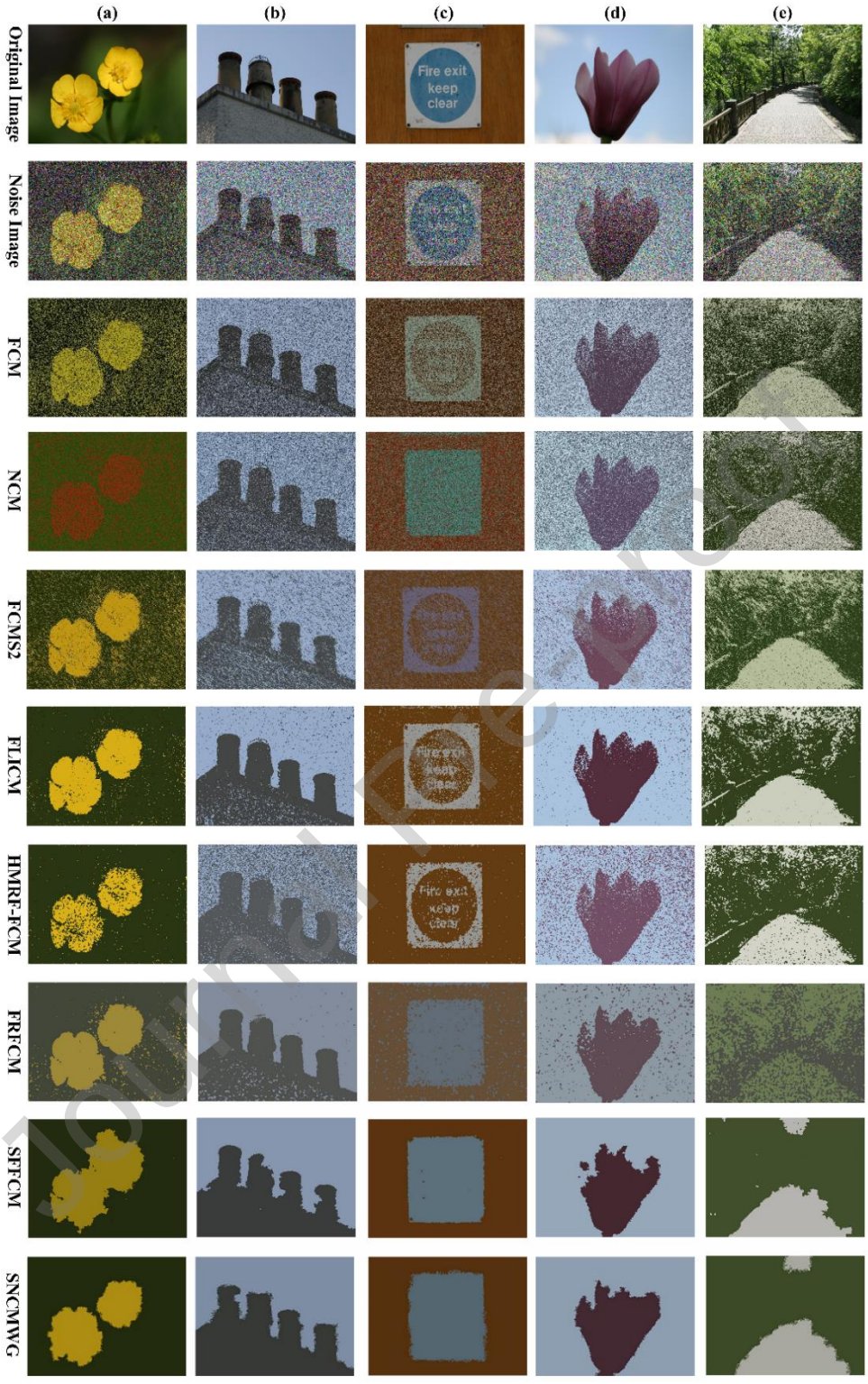

Fig. 16. Comparison on of segmentation results on the different mixed noise images.

5. Conclusion

In this paper, a spuerpixel-neutrosophic C-means clustering with gradient-based structural similarity is proposed for color image segmentation. The SLIC algorithm combines multiple morphological reconstructions to obtain accurate target contours. While maintaining the target contour, the number of clusters is reduced. In addition, the adaptive neighborhood information is added to the NCM algorithm, and then the improved NCM algorithm obtains more a precise definition of uncertain superpixels.

Meantime, the similarity is used to classify these superpixels instead of the maximum membership rule, which solves the problem of misclassification and destruction of global spatial information caused by only relying on Euclidean distance for some superpixels. Experimental results show that this method can correctly and effectively segment images either clean or noise.

But the SLIC algorithm must set the number of superpixels in advance, which has limitations in practical applications. In future work, we will explore a neutrosophic clustering algorithm that automatically estimates the number of cluster centers and the number of superpixels.

Appendices A

In Appendix A, the derivation process of SNCM is described in detail.

The objective function of Superpixel-neutrosophic C-means clustering is:

$$J(T,I,F,c)=\sum_{l=1}^{q}\sum_{k=1}^{\mathrm{C}} S_l\left(w_1 T_{kl}\right)^m \left\|\left(\frac{1}{S_l}\sum_{p\in R_l} x_p - c_k\right)\right\|^2 + \sum_{l=1}^{q} S_l\left(w_2 I_l\right)^m \left\|\left(\frac{1}{S_l}\sum_{p\in R_l} x_p - c_{l\max}\right)\right\|^2 + \sum_{l=1}^{q} S_l\left(w_3 F_l\right)^m \delta^2 \tag{A.1}$$

$$\delta^2 = \gamma \frac{\sum_{l=1}^{q}\sum_{k=1}^{C}\left\|\left(\frac{1}{S_l}\sum_{p\in R_l} x_p - c_k\right)\right\|^2}{qC} \tag{A.2}$$

Where l is the color level, $1\le l\le q$, q is the number of regions of the superpixel image, c_k is the cluster center, S_l is the number of pixels in the lth superpixel R_l, and x_p is the color pixel within the lth superpixel R_l, δ is a noise distance calculated by Eq.(11). T_{kl}, I_l and F_i are the membership values belonging to the determinate cluster, boundary regions and noisy data set, $0<T_{kl},I_l,F_l<1$ which satisfy with the following:

$$\sum_{k=1}^{C} T_{kl} + I_l + F_l = 1 \tag{A.3}$$

According to the above formula, the Lagrange objective function is constructed as:

$$L(T,I,F,c,\lambda)=\sum_{l=1}^{q}\sum_{k=1}^{\mathrm{C}} S_l\left(w_1 T_{kl}\right)^m \left\|\left(\frac{1}{S_l}\sum_{p\in R_l} x_p - c_k\right)\right\|^2 + \sum_{l=1}^{q} S_l\left(w_2 I_l\right)^m \left\|\left(\frac{1}{S_l}\sum_{p\in R_l} x_p - c_{l\max}\right)\right\|^2 + \sum_{l=1}^{q} S_l\left(w_3 F_l\right)^m \delta^2 - \sum_{l=1}^{q}\lambda_l\left(\sum_{k=1}^{c} T_{kl} + I_l + F_l - 1\right) \tag{A.4}$$

Where λ is a Lagrange multiplier to minimize the Lagrange objective function, we use the following operations:

$$\frac{\partial L}{\partial T_{kl}} = mS_l \left(w_1 T_{kl}\right)^{m-1} \left\| \left(\frac{1}{S_l} \sum_{p \in R_l} x_p - c_k \right) \right\|^2 - \lambda_l \tag{A.5}$$

$$\frac{\partial L}{\partial I_l} = mS_l \left(w_2 I_l\right)^{m-1} \left\| \left(\frac{1}{S_l} \sum_{p \in R_l} x_p - c_{l\max} \right) \right\|^2 - \lambda_l \tag{A.6}$$

$$\frac{\partial L}{\partial F_l} = mS_l \left(w_3 F_l\right)^{m-1} \delta^2 - \lambda_l \tag{A.7}$$

$$\frac{\partial L}{\partial c_k} = -2\sum_{l=1}^{q} S_l \left(w_1 T_{kl}\right)^{m} \left\| \left(\frac{1}{S_l} \sum_{p \in R_l} x_p - c_k \right) \right\| \tag{A.8}$$

The norm is specified as the Euclidean norm. Let $\partial L/\partial T_{kl} = 0$, $\partial L/\partial I_l = 0$, $\partial L/\partial F_l = 0$ and $\partial L/\partial c_k = 0$, then

$$T_{kl} = \frac{1}{w_1} \left(\frac{\lambda_l}{mS_l} \right)^{1/m-1} \left(\frac{1}{S_l} \sum_{p \in R_l} x_p - c_k \right)^{-(2/m-1)} \tag{A.9}$$

$$I_l = \frac{1}{w_2} \left(\frac{\lambda_l}{mS_l} \right)^{1/m-1} \left(\frac{1}{S_l} \sum_{p \in R_l} x_p - c_{l\max} \right)^{-(2/m-1)} \tag{A.10}$$

$$F_l = \frac{1}{w_3} \left(\frac{\lambda_l}{mS_l} \right)^{1/m-1} \left(\delta \right)^{-(2/m-1)} \tag{A.11}$$

$$c_k = \frac{\sum_{l=1}^{q} \left(w_1 T_{kl}\right)^m \sum_{p \in R_l} x_p}{\sum_{l=1}^{q} S_l \left(w_1 T_{kl}\right)^m} \tag{A.12}$$

Let $\left(\frac{\lambda_l}{mS_l} \right)^{1/m-1} = K$, then

$$\sum_{k=1}^{C} \frac{K}{w_1} \left\| \left(\frac{1}{S_l} \sum_{p \in R_l} x_p - c_k \right) \right\|^{-(2/m-1)} + \frac{K}{w_2} \left\| \left(\frac{1}{S_l} \sum_{p \in R_l} x_p - c_{l\max} \right) \right\|^{-(2/m-1)} + \frac{K}{w_3} \delta^{-(2/m-1)} = 1 \tag{A.13}$$

$$K = \left[\sum_{k=1}^{C} \frac{1}{w_1} \left\| \left(\frac{1}{S_l} \sum_{p \in R_l} x_p - c_k \right) \right\|^{-(2/m-1)} + \frac{1}{w_2} \left\| \left(\frac{1}{S_l} \sum_{p \in R_l} x_p - c_{l\max} \right) \right\|^{-(2/m-1)} + \frac{1}{w_3} \delta^{-(2/m-1)} \right]^{-1} \tag{A.14}$$

Therefore,

$$T_{kl} = \frac{K}{w_1} \left(\frac{1}{S_l} \sum_{p \in R_l} x_p - c_k \right)^{-(2/m-1)} \tag{A.15}$$

$$I_l = \frac{K}{w_2}\left(\frac{1}{S_l}\sum_{p\in R_l} x_p - c_{l\max}\right)^{-(2/m-1)} \quad \text{(A.16)}$$

$$F_l = \frac{K}{w_3}\delta^{-(2/m-1)} \quad \text{(A.17)}$$

Acknowledgments

This work is supported by the grant of the Academic Natural Science Research Project of AnHui No.KJ2020A0250.

References

[1] Yanhui Guo, Abdulkadir Şengür, Yaman Akbulut, Abriel Shipley. An Effective Color Image Segmentation Approach Using Neutrosophic Adaptive Mean Shift Clustering[J]. Measurement, 2018, 119:28-40.

[2] M. Q. Li, L. P. Xu, Shan Gao, Na Xu, and Bo Yan, "Remote sensing image segmentation based on a robust fuzzy C-means algorithm improved by a parallel Lévy greywolf algorithm," Appl. Opt. 58, 4812-4822 (2019).

[3] Mohamed Abd Elaziz, Neggaz Nabil, Reza Moghdani, Ahmed A. Ewees, Erik Cuevas & Songfeng Lu. Multilevel thresholding image segmentation based on improved volleyball premier league algorithm using whale optimization algorithm. Multimed Tools Appl 80, 12435–12468 (2021).

[4] Asma Touil, Karim Kalti, Pierre-Henri Conze, Basel Solaiman & Mohamed Ali Mahjoub. A new conditional region growing approach for microcalcification delineation in mammograms. Med Biol Eng Comput 59, 1795–1814 (2021).

[5] Guotai Wang, Maria A. Zuluaga, Wenqi Li, Rosalind Pratt, Premal A. Patel, Michael Aertsen, Tom Doel, Anna L. David, Jan Deprest, Sébastien Ourselin, Tom Vercauteren, "DeepIGeoS: A Deep Interactive Geodesic Framework for Medical Image Segmentation," in IEEE Transactions on Pattern Analysis and Machine Intelligence, vol. 41, no. 7, pp. 1559-1572, 1 July 2019.

[6] Isabelle Bloch. Fuzzy sets for image processing and understanding[J]. Fuzzy Sets and Systems, 2015, 281(C):280-291.

[7] MacQueen, James. "Some methods for classification and analysis of multivariate observations." In Proceedings of the fifth Berkeley symposium on mathematical statistics and probability, vol. 1, no. 14, pp. 281-297. 1967.

[8] Le Hoang Son, Bui Cong Cuong, Pier Luca Lanzi, Nguyen Tho Thong. A novel intuitionistic fuzzy clustering method for geo-demographic analysis[J]. Expert Systems with Applications,2012,39(10):9848-9859.

[9] von Luxburg, U. A tutorial on spectral clustering. Stat Comput 17, 395–416 (2007).

[10] BEZDEK J C.Pattern recognition with fuzzy objective function algoritms[M]. NewYork;Plenum Press,1981.

[11] ALI M A. Image segmentation: A fuzzy clustering framework[M].Saarbrucken,German: VDM Verlag Dr.Miller,2010.

[12] M. N. Ahmed, S. M. Yamany, N. Mohamed, A. A. Farag and T. Moriarty, "A modified fuzzy c-means algorithm for bias field estimation and segmentation of MRI data," in IEEE Transactions on Medical Imaging, vol. 21, no. 3, pp. 193-199, March 2002.

[13] Songcan Chen and Daoqiang Zhang, "Robust image segmentation using FCM withspatial constraints based on new kernel-induced distance measure," in IEEE Transactions on Systems, Man, and Cyberne

tics, Part B (Cybernetics), vol. 34, no. 4, pp. 1907-1916, Aug. 2004.
[14] S. P. Chatzis and T. A. Varvarigou, "A Fuzzy Clustering Approach Toward Hidden Markov Rando m Field Models for Enhanced Spatially Constrained Image Segmentation," in IEEE Transactions on Fuz zy Systems, vol. 16, no. 5, pp. 1351-1361, Oct. 2008.
[15] S. Krinidis and V. Chatzis, "A Robust Fuzzy Local Information C-Means Clustering Algorithm," in IEEE Transactions on Image Processing, vol. 19, no. 5, pp. 1328-1337, May 2010.
[16] T. Lei, X. Jia, Y. Zhang, L. He, H. Meng and A. K. Nandi, "Significantly Fast and Robust Fuzzy C-Means Clustering Algorithm Based on Morphological Reconstruction and Membership Filtering," in IEEE Transactions on Fuzzy Systems, vol. 26, no. 5, pp. 3027-3041, Oct. 2018.
[17] T. Lei, X. Jia, Y. Zhang, S. Liu, H. Meng and A. K. Nandi, "Superpixel-Based Fast Fuzzy C-Mea ns Clustering for Color Image Segmentation," in IEEE Transactions on Fuzzy Systems, vol. 27, no. 9, pp. 1753-1766, Sept. 2019.
[18] F. Smarandache, A Unifying Field in Logics Neutrosophic Logic. Neutrosophy, Neutrosophic Set, N eutrosophic Probability, third ed., American Research Press, 2003.
[19] Yanhui Guo and Abdulkadir Sengur. "NCM: Neutrosophic c -means clustering algorithm". Pattern Recognition 48.8(2015): 2710-2724..
[20] Yanhui Guo, Rong Xia, Abdulkadir Şengür & Kemal Polat. A novel image segmentation approach based on neutrosophic c-means clustering and indeterminacy filtering. Neural Comput & Applic 28, 300 9–3019 (2017).
[21] R. Achanta, A. Shaji, K. Smith, A. Lucchi, P. Fua and S. Süsstrunk, "SLIC Superpixels Compared to State-of-the-Art Superpixel Methods," in IEEE Transactions on Pattern Analysis and Machine Intelli gence, vol. 34, no. 11, pp. 2274-2282, Nov. 2012.
[22] Achanta R, Shaji A, Smith K, Lucchi A, Fua P, Süsstrunk S. Slic superpixels. No. REP_WORK. 2010..
[23] Zhenyu Lu and Yunan Qiu and Tianming Zhan. Neutrosophic C-means Clustering with Local Infor mation and Noise Distance-based Kernel Metric Image Segmentation[J].Journal of Visual Communication and Image Representation, 2018, 58 : 269-276.
[24] SANG, Qing-bing, Di-lin LIANG, Xiao-jun WU, and Chao-feng LI. "Gradient Structural Similarity Image Assessment Index Based on Dilation." Computer Science (2014).
[25] Hore, Alain, and Djemel Ziou. "Image quality metrics: PSNR vs. SSIM." In 2010 20th internationa l conference on pattern recognition, pp. 2366-2369. IEEE, 2010.
[26] M.S. Yang, Convergence properties of the generalized fuzzy c-means clustering algorithms, Comput. Math. Appl. 25 (12) (1993) 3–11.
[27] Qijian Zhang, Runmin Cong, Chongyi Li, Ming-Ming Cheng, Yuming Fang, Xiaochun Cao, Yao Z hao, and Sam Kwong, Dense attention fluid network for salient object detection in optical remote sensi ng images, IEEE Transactions on Image Processing, vol. 30, pp. 1305-1317, 2021.
[28] P. Arbeláez, M. Maire, C. Fowlkes and J. Malik, "Contour Detection and Hierarchical Image Segm entation," in IEEE Transactions on Pattern Analysis and Machine Intelligence, vol. 33, no. 5, pp. 898-9 16, May 2011.
[29] J. Shotton, J. Winn, C. Rother and A. Criminisi, “Textonboost: joint appearance, shape and context modeling for multi-class object recognition and segmentation,” in Proc.Eur. Conf. Comput. Vis. (ECC V), Graz, Austria, 2006, pp. 1-15.
[30] R. Unnikrishnan, C. Pantofaru and M. Hebert, "Toward Objective Evaluation of Image Segmentatio n Algorithms," in IEEE Transactions on Pattern Analysis and Machine Intelligence, vol. 29, no. 6, pp.

929-944, June 2007.
[31] X. Wang, Y. Tang, S. Masnou and L. Chen, "A Global/Local Affinity Graph for Image Segmentati on," in IEEE Transactions on Image Processing, vol. 24, no. 4, pp. 1399-1411.

Declaration of interests

☒The authors declare that they have no known competing financial interests or personal relationships that could have appeared to influence the work reported in this paper.

☐The authors declare the following financial interests/personal relationships which may be considered as potential competing interests: